IAC-22-71028

Numerically Efficient Methods For Low-Thrust Collision Avoidance Meneuvers Design in GEO Regime

Alexia Cantoni[a]*, Andrea De Vittori[b], Pierluigi Di Lizia[c], Roberto Armellin[d]

[a] Department of Aerospace Engineering, Politecnico di Milano, Via Privata Giuseppe La Masa 34, Milano, Lombardia, Italia 20156, alexia.cantoni@mail.polimi.it
[b] Department of Aerospace Engineering, Politecnico di Milano, Via Privata Giuseppe La Masa 34, Milano, Lombardia, Italia 20156, andrea.devittori@polimi.it
[c] Department of Aerospace Engineering, Politecnico di Milano, Via Privata Giuseppe La Masa 34, Milano, Lombardia, Italia 20156, pierluigi.dilizia@polimi.it
[d] Department of Aerospace Engineering, University of Auckland, 20 Symonds Street, Auckland Central, Auckland, New Zealand 1010, roberto.armellin@auckland.ac.nz

* Corresponding Author

Abstract

The rapid growth of the space debris population is leading to an uptick in satellite proximity events.

The Geostationary Orbit (GEO) region is less populated than the Low Earth Orbit (LEO) regime, but the debris density is still significant despite the difference in the absolute number of satellites belonging to the two regions. In particular, the increasing number of spacecraft reaching their end-of-life and the existing debris, such as rocket bodies, could threaten operative satellites and require onboard Collision Avoidance Maneuver (CAM) planning down the road. Moreover, in this peculiar regime, spacecraft are subjected to gravitational perturbations that cause satellites to cross the assigned geostationary slot delimited by sharp latitude and longitude limits. To overcome this issue, ad-hoc control strategies are adopted to keep the spacecraft within specified boundaries through station-keeping maneuvers. Currently, the state-of-the-art treats CAMs and station-keeping as separate problems. This paper illustrates how to embed both with an analytical and a time-efficient policy designed for low-thrust propulsion systems. First, an extension of previous similar work in LEO has been carried out to GEO considering a pure Keplerian motion. Several firing strategies have been: the North-South and East-West energy-optimal maneuvers, typical of station-keeping. Then, with the inclusion of geopotential perturbation in the CAM design, a station-keeping maneuver has been formulated as a Multi-Point Boundary Value Problem (MPBVP) with specific constraints on Probability of Collision (PoC) at Time of Closest Approach (TCA) and final state. The idea is to leverage the motion linearization with the state transition matrix (STM) and transform the energy-optimal control problem into an Initial Value Problem. In particular, the problem-solution can distinguish between two possible scenarios. On one hand, station-keeping alone is enough to ensure a PoC lower than a safeguard limit. On the other, when not fulfilling this requirement, the algorithm autonomously identifies the best strategy for commanding CAM and station-keeping by imposing an arbitrary PoC at TCA. Results show a reduced computational time burden suitable for onboard CAM planning and a decreasing Δv for longer maneuvering times.

Keywords: CAM, GEO, MPBVP, PoC, collision

Nomenclature

R	Rotation matrix
b	Position vector in the B-Plane Reference
r	Position vector in the ECI Reference
v	Velocity Vector in the ECI Reference
a	Acceleration vector
Φ	State Transition Matrix
x	State vector
A	State matrix
J	Cost function
Ψ	Terminal function for the TPBVP
a	Scalar acceleration
$\boldsymbol{\epsilon}$	Control direction
ϵ	Weighting factor
H	Hamiltonian
$\boldsymbol{\lambda}$	Costate vector
μ	Earth gravitational constant
ν	Multiplier for equality condition in the TPBVP
u	Vector direction
γ	Terminal function fo the MPBVP
Φ	Angular deviation between ECI and ECEF
k	Multiplier for the inequality condition in the MPBVP

Acronyms/Abbreviations

CAM	Collision Avoidance Maneuver
ECI	Earth Centered Inertial reference frame
EOP	Energy Optimal Control Problem
GEO	Geostationary Earth Orbit

EGO	Extended Geostationary Orbit
IVP	Initial Value Problem
LEO	Low Earth Orbit
MPBVP	Multi-Point Boundary Value Problem
OCP	Optimal Control Problem
PoC	Probability of Collision
SMD	Squared Mahalanobis Distnace
STM	State Transition Matrix
TCA	Time of Closest Approach
TPBVP	Two Point Boundary Balue Problem

1. Introduction

Since space activity started, the number of human-made objects around the Earth has progressively increased. As the congestion grows, so too have close calls between orbiting assets, causing an uptick in full-on collisions to be reckoned in any space mission.

Among all the orbital regimes, the Geostationary environment is exploited for many space and commercial applications. However, natural mechanisms for spacecraft removal in this regime are not available. Consequently, the debris population is skyrocketing, with sizes ranging from small explosion fragments to rocket upper stages. Regrettably, only the largest objects are regularly observed and catalogued, while the smallest cannot be detected. Given the alarming situation, sustainable use of space can be reached following international guidelines and standards [1]. Among them, this work focuses on computationally efficient Collision Avoidance Maneuvers (CAMs) in GEO to make a step forward to onboard planning.

During CAM design, the Probability of Collision (PoC) and the required Δv are minimized. One peculiar aspect of the GEO regime is the satellite slot allocation defined by sharp latitude and longitude values, also called station-keeping boxes, for the entire operative life. For this reason, satellites are forced to frequently perform station-keeping cycles to counteract the perturbation effects on their nominal orbits. Bearing in mind none of the current existing strategies for the maneuver execution includes station-keeping, this work initially addresses analytical CAMs with a formulation stemming from [2] , further extended with North-South and East-West firing directions. To strictly comply with slot constraints, a Multi-Point Boundary Value Problem (MPBVP) is first thought to satisfy both the PoC condition and the targeted final state with two separate Optimal Control Problems (OCPs), later improved with a single OCP formulation, still featuring an analytical formulation.

1. Fundamentals

This section describes the theoretical background needed for the analytical CAM formulation.

1.1. Conjunction definition

The CAM design process considers the short-term encounter between a satellite and debris. The controllable object (called primary) is described by a state $\boldsymbol{x}_p = [\boldsymbol{r}_p,\ \boldsymbol{v}_p]^\mathsf{T}$ while the piece of debris (secondary object) is identified by the state $\boldsymbol{x}_s = [\boldsymbol{r}_s,\ \boldsymbol{v}_s]^\mathsf{T}$. $\boldsymbol{r}_i$ and $\boldsymbol{v}_i$ are the position and the velocity of the centre of mass of the single object measured in a generic reference $\hat{R}$.

For collision probability computation, a valuable coordinate rf. is the B-Plane. The origin lies at the centre of the secondary object at the time of closest approach, as depicted in Fig. 1 with the following axes direction:

$$\boldsymbol{u}_\xi = \frac{\boldsymbol{v}_p \times \boldsymbol{v}_s}{\left|\left|\boldsymbol{v}_p \times \boldsymbol{v}_s\right|\right|}, \boldsymbol{u}_\eta = \frac{\boldsymbol{v}_p - \boldsymbol{v}_s}{\left|\left|\boldsymbol{v}_p - \boldsymbol{v}_s\right|\right|}, \quad \boldsymbol{u}_\zeta = \boldsymbol{u}_\xi \times \boldsymbol{u}_\eta \tag{1}$$

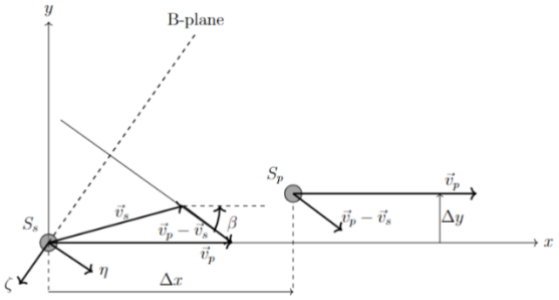

Fig. 1: BPlane reference frame source [2]

Consequently, the position vector in the B-Plane reference frame is identified as $\boldsymbol{b}_{3D} = [\xi, \eta, \zeta]^\mathsf{T}$. The rotation matrix to pass from the inertial reference to the B-Plane one is defined as:

$$\boldsymbol{R}_{b,3D} = \left[\boldsymbol{u}_\xi, \boldsymbol{u}_\eta, \boldsymbol{u}_\zeta\right]^\mathsf{T} \tag{2}$$

Additionally, the projection on the η axis is given by:

$$\boldsymbol{R}_{b,2D} = \left[\boldsymbol{u}_\xi, \boldsymbol{u}_\zeta\right]^\mathsf{T} \tag{3}$$

Consequently, the 2D position vector in the B-Plane is defined as $\boldsymbol{b} = [\xi, \zeta]^\mathsf{T}$.

1.2. Chan's PoC model

PoC between the primary and secondary objects, experiencing short-term conjunction, can be obtained by integrating the relative position probability density function over a sphere of radius R_A (i.e. the hard body sphere given by the summed primary and secondary radii) at TCA. This assumption is made up for the lack of information about attitude and geometry, especially true for the secondary object [3]. Assuming that the relative probability distribution function is Gaussian, an approximated collision probability is obtained with the Chan's method of equivalent cross-sectional areas:

$$\mathrm{PoC}(u,v) = e^{-\frac{v}{2}} \sum_{m=0}^{\infty} \frac{v^m}{2^m m!} \left[1 - e^{-\frac{u}{2}} \sum_{k=0}^{m} \frac{u^k}{2^k k!} \right] \tag{4}$$

Where u is the ratio of the impact cross-sectional area to the 1σ B-Plane covariance ellipse area:

$$u = \frac{s_A^2}{\sigma_\xi \sigma_\zeta \sqrt{1-\rho_{\xi\zeta}^2}} \tag{5}$$

and v is the Squared Mahalanobis Distance (SMD):

$$\boldsymbol{v} = \frac{\left(\frac{\xi}{\sigma_\xi}\right)^2 + \left(\frac{\zeta}{\sigma_\zeta}\right)^2 - 2\rho_{\xi\zeta}\frac{\xi}{\sigma_\xi}\frac{\zeta}{\sigma_\zeta}}{1-\rho_{\xi\zeta}^2} = \\ = \left(\boldsymbol{r}_p - \boldsymbol{r}_s\right)^\top \boldsymbol{R}_{b,2D}^\top C^{-1} \boldsymbol{R}_{b,2D} \left(\boldsymbol{r}_p - \boldsymbol{r}_s\right) = \boldsymbol{b}_p^\top C^{-1} \boldsymbol{b}_p \tag{6}$$

where: $\boldsymbol{C}$ is the covariance matrix, and $\boldsymbol{b}_p$ is the primary object position relative to the secondary object in the B-Plane framework.

1.3. Dynamics

The dynamics of space objects in the approximation of a two-body encounter can be formulated in terms of the equation of motion:

$$\ddot{\boldsymbol{r}} = -\frac{\mu}{r^3}\boldsymbol{r} \tag{7}$$

where $\boldsymbol{r}$ is the object position in ECI reference. Developing this equation in a state matrix form, and introducing the control acceleration $\boldsymbol{a}_c$ the two-body dynamics can be rewritten as:

$$\begin{cases} \dot{\boldsymbol{r}} = \boldsymbol{v} \\ \dot{\boldsymbol{v}} = -\frac{\mu}{r^3}\boldsymbol{r} + \boldsymbol{a}_c \end{cases} \tag{8}$$

This model can be used as a first approximation to describe the motion of a satellite around the Earth. For a more refined CAM design in GEO, the geopotential perturbation is encompassed as it is the main responsible for deviating a satellite from the nominal trajectory.

Specifically, the associated power series is expanded up to the J_{22} term. Therefore, the system dynamics becomes:

$$\begin{cases} \dot{\boldsymbol{r}} = \boldsymbol{v} \\ \dot{\boldsymbol{v}} = -\frac{\mu}{r^3}\boldsymbol{r} + \boldsymbol{a}_c + \boldsymbol{a}_{geo} \end{cases} \tag{9}$$

where $\boldsymbol{a}_{geo} = f(r,\psi,\lambda)$, r is the radial distance, ψ is the geocentric latitude, and λ is the geocentric longitude in polar coordinates (for the $\boldsymbol{a}_{geo}$ evaluation see [4].

1.4. State Transition Matrix

Given the non-linear dynamics described in the previous section, the State Transition Matrix (STM) labelled as $\boldsymbol{\Phi}$ allows to map an arbitrary state variation with respect to a nominal trajectory (for CAMs the ballistic motion) from a certain time t_0 to t_f according to the following equation:

$$\delta \boldsymbol{x}_f = \boldsymbol{\Phi} \delta \boldsymbol{x}_0 \tag{10}$$

For time-varying systems, $\boldsymbol{\Phi}(t,t_0)$ can be found by integrating the following set of differential equations:

$$\dot{\boldsymbol{\Phi}}(t,t_0) = \boldsymbol{A}(t)\boldsymbol{\Phi}(t,t_0), \boldsymbol{\Phi}(t_0,t_0) = \boldsymbol{I} \tag{11}$$

where $\boldsymbol{\Phi}(t_0,t_0)$ is the initial condition and $\boldsymbol{A}(t)$ is the state matrix of the dynamical system $\boldsymbol{f}(\boldsymbol{x},t)$ around the nominal trajectory $\boldsymbol{x}_n$:

$$\boldsymbol{A} = \frac{\partial \boldsymbol{f}(\boldsymbol{x},t)}{\partial \boldsymbol{x}}\Big|_{x_n} \tag{12}$$

2. Energy-Optimal CAM for free, E-W and N-S thrust directions

The main objective of CAMs is to minimize both the PoC and the propellant consumption through the definition of a cost function J:

$$J = \nu \Psi(\boldsymbol{x}(t_{TCA}), t_{TCA}) + \\ + \int_{t_0}^{t_{TCA}} \frac{1}{2} a_{max} \boldsymbol{\epsilon}^\top \boldsymbol{\epsilon} dt \tag{13}$$

where: Ψ represents the equality constraint on the SMD at the final maneuvering time (t_{TCA}), $\boldsymbol{a}_{max}$ is the maximum value of control acceleration, imposed equal to $8 \cdot 10^{-7}\ km/s^2$ (compatible with a typical low-thrust propulsion technology), and $\boldsymbol{\epsilon}$ is a weighting factor. That said, the energy optimal policy may exceed the thruster capabilities being the control unbounded.

This section focuses on the formulation of the Energy Optimal Control Problem (EOP) applicable to different scenarios: free-thrust direction is considered first, then the North-South and East-west forced directions are investigated without including the J_{22} term. Notably, the control acceleration strictly depends on the initial maneuvering point and on the targeted SMD. An approach already proposed for the LEO regime in [2] is extended here to the Geostationary orbits.

For the free direction firing the acceleration is found by setting $\frac{\partial H}{\partial \epsilon} = 0$, where H is the Hamiltonian function:

$$\boldsymbol{a}_c = -a_{max}\boldsymbol{\lambda}_v \tag{14}$$

The aim of the problem is to transform the resulting Two Point Boundary Value Problem (TPBVP), obtained by way of the Euler-Lagrange equations:

$$\begin{cases} \dot{\boldsymbol{r}} = \boldsymbol{v} \\ \dot{\boldsymbol{v}} = -\frac{\mu}{r^3}\boldsymbol{r} - a_{max}\boldsymbol{\lambda}_v \\ \dot{\boldsymbol{\lambda}}_r = \frac{\mu}{r^3}\boldsymbol{\lambda}_v - \frac{3\mu \boldsymbol{r}\cdot\boldsymbol{\lambda}_v}{r^5}\boldsymbol{r} \\ \dot{\boldsymbol{\lambda}}_v = -\boldsymbol{\lambda}_r \end{cases} \quad \begin{cases} \boldsymbol{r}(t_0) = \boldsymbol{r}_0^m \\ \boldsymbol{v}(t_0) = \boldsymbol{v}_0^m \\ \boldsymbol{\lambda}_r(t_{TCA}) = \nu 2\boldsymbol{R}_{b,2D}^{\top}\boldsymbol{C}^{-1}\boldsymbol{R}_{b,2D}(\boldsymbol{r}_{TCA}^m - \boldsymbol{r}_s) \\ \boldsymbol{\lambda}_v(t_{TCA}) = \boldsymbol{0} \end{cases} \tag{15}$$

into an Initial Value Problem (IVP) with unknown $\boldsymbol{\lambda}_{r_0}^m$ and $\boldsymbol{\lambda}_{v_0}^m$:

$$\begin{cases} \dot{\boldsymbol{r}} = \boldsymbol{v} \\ \dot{\boldsymbol{v}} = -\frac{\mu}{r^3}\boldsymbol{r} - a_{max}\boldsymbol{\lambda}_v \\ \dot{\boldsymbol{\lambda}}_r = \frac{\mu}{r^3}\boldsymbol{\lambda}_v - \frac{3\mu \boldsymbol{r}\cdot\boldsymbol{\lambda}_v}{r^5}\boldsymbol{r} \\ \dot{\boldsymbol{\lambda}}_v = -\boldsymbol{\lambda}_r \end{cases} \quad \begin{cases} \boldsymbol{r}(t_0) = \boldsymbol{r}_0^m \\ \boldsymbol{v}(t_0) = \boldsymbol{v}_0^m \\ \boldsymbol{\lambda}_r(t_0) = \boldsymbol{\lambda}_{r_0}^m \\ \boldsymbol{\lambda}_v(t_0) = \boldsymbol{\lambda}_{v_0}^m \end{cases} \tag{16}$$

The superscript m stands for maneuverer, and it indicates the controlled trajectory. According to the approach described in Sect. 1.4, IVP solves by computing the STM to link the initial state and costates variation:

$$\begin{aligned} &\delta\boldsymbol{x}_0 = \\ &\left[\boldsymbol{r}_0^m - \boldsymbol{r}_0,\ \boldsymbol{v}_0^m - \boldsymbol{v}_0,\ \boldsymbol{\lambda}_{r_0}^m - \boldsymbol{\lambda}_{r_0},\ \boldsymbol{\lambda}_{v_0}^m - \boldsymbol{\lambda}_{v_0}\right]^{\top} = \\ &\qquad = \left[\boldsymbol{0},\ \boldsymbol{0},\ \delta\boldsymbol{\lambda}_{r_0},\ \delta\boldsymbol{\lambda}_{v_0}\right]^{\top} \end{aligned} \tag{17}$$

to the final ones:

$$\begin{aligned} &\delta\boldsymbol{x}_{TCA} = \\ &\left[\boldsymbol{r}_{TCA}^m - \boldsymbol{r}_{TCA},\ \boldsymbol{v}_{TCA}^m - \boldsymbol{v}_{TCA},\ \boldsymbol{\lambda}_{r_{TCA}}^m - \boldsymbol{\lambda}_{r_{TCA}},\ \boldsymbol{\lambda}_{v_{TCA}}^m - \boldsymbol{\lambda}_{v_{TCA}}\right]^{\top} = \\ &\qquad = \left[\delta\boldsymbol{r}_{TCA},\ \delta\boldsymbol{v}_{TCA},\ \delta\boldsymbol{\lambda}_{r_{TCA}},\ \boldsymbol{0}\right]^{\top} \end{aligned} \tag{18}$$

In this way:

$$\delta\boldsymbol{x}_{TCA} = \boldsymbol{\Phi}\delta\boldsymbol{x}_0 \tag{19}$$

$$\boldsymbol{\Phi} = \begin{bmatrix} \boldsymbol{\phi}_{11} & \boldsymbol{\phi}_{12} & \boldsymbol{\phi}_{13} & \boldsymbol{\phi}_{14} \\ \boldsymbol{\phi}_{21} & \boldsymbol{\phi}_{22} & \boldsymbol{\phi}_{23} & \boldsymbol{\phi}_{24} \\ \boldsymbol{\phi}_{31} & \boldsymbol{\phi}_{32} & \boldsymbol{\phi}_{33} & \boldsymbol{\phi}_{34} \\ \boldsymbol{\phi}_{41} & \boldsymbol{\phi}_{42} & \boldsymbol{\phi}_{43} & \boldsymbol{\phi}_{44} \end{bmatrix} \tag{20}$$

$\boldsymbol{\phi}_{i,j}$ is a 3x3 matrix. This notation helps in the solution scheme for the presented methods. First, express $\delta\boldsymbol{\lambda}_{r_0}$ and $\delta\boldsymbol{\lambda}_{v_0}$, with the third and the fourth rows of Eq. (19), as a function of $\delta\boldsymbol{\lambda}_{r_{TCA}}$:

$$\begin{aligned} \delta\boldsymbol{\lambda}_{v_0} &= -\boldsymbol{\phi}_{44}^{-1}\boldsymbol{\phi}_{43}\boldsymbol{B}^{-1}\delta\boldsymbol{\lambda}_{r_{TCA}} \\ \delta\boldsymbol{\lambda}_{r_0} &= \boldsymbol{B}^{-1}\delta\boldsymbol{\lambda}_{r_{TCA}} \end{aligned} \tag{21}$$

Where:

$$\boldsymbol{B} = \boldsymbol{\phi}_{33} - \boldsymbol{\phi}_{34}\boldsymbol{\phi}_{44}^{-1}\boldsymbol{\phi}_{43} \tag{22}$$

Using the first row of Eq. (19):

$$\delta\boldsymbol{r}_{TCA} = \boldsymbol{D}\delta\boldsymbol{\lambda}_{v_0} = \boldsymbol{D}\boldsymbol{B}^{-1}\delta\boldsymbol{\lambda}_{r_{TCA}} \tag{23}$$

the condition on $\boldsymbol{\lambda}_r(t_{TCA})$ from Eq. (15), and the SMD constraint from Eq. (6) leads to the following system in 4 equations and in 4 unknowns ($\boldsymbol{r}_{TCA}^m$ and ν):

$$\begin{cases} \delta\boldsymbol{r}_{TCA} = 2\nu\boldsymbol{D}\boldsymbol{B}^{-1}\boldsymbol{Q}\boldsymbol{R}_{b,2D}(\boldsymbol{r}_{TCA}^m - \boldsymbol{r}_s) \\ (\boldsymbol{r}_{TCA}^m - \boldsymbol{r}_s)^{\top}\boldsymbol{R}_{b,2D}^{\top}\boldsymbol{Q}\boldsymbol{R}_{b,2D}(\boldsymbol{r}_{TCA}^m - \boldsymbol{r}_s) = \overline{SMD} \end{cases} \tag{24}$$

Where:

$$\boldsymbol{D} = \boldsymbol{\phi}_{13} - \boldsymbol{\phi}_{14}\boldsymbol{\phi}_{44}^{-1}\boldsymbol{\phi}_{43} \tag{25}$$

By left-multiplying both sides of the first equation of Eq. (24) by $\boldsymbol{R}_{b,2D}$, subtracting and adding $\boldsymbol{r}_s$ to its L.H.S it leads to:

$$\begin{cases} \boldsymbol{b}_p^m - \boldsymbol{b}_p = 2\nu\boldsymbol{D}\boldsymbol{B}^{-1}\boldsymbol{Q}\boldsymbol{b}_p^m \\ \boldsymbol{b}_p^{m\top}\boldsymbol{Q}\boldsymbol{R}_{b,2D}\boldsymbol{b}_p^m = \overline{SMD} \end{cases} \tag{26}$$

With:

$$\begin{aligned} \boldsymbol{b}_p &= \boldsymbol{R}_{b,2D}(\boldsymbol{r}_{TCA} - \boldsymbol{r}_s) \\ \boldsymbol{b}_p^m &= \boldsymbol{R}_{b,2D}(\boldsymbol{r}_{TCA}^m - \boldsymbol{r}_s) \end{aligned} \tag{27}$$

Appropriate manipulation of these outputs the following fourth-order polynomial equation in the variable ν:

$$\nu^2\left(\tilde{\boldsymbol{E}}\boldsymbol{b}_p\right)^{\top}\boldsymbol{Q}\left(\tilde{\boldsymbol{E}}\boldsymbol{b}_p\right) - \nu\left[\boldsymbol{b}_p^{\top}\boldsymbol{Q}\tilde{\boldsymbol{E}}\boldsymbol{b}_p + \left(\boldsymbol{E}\boldsymbol{b}_p\right)^{\top}\boldsymbol{b}_p\right] = \overline{SMD}\,det(I-\nu\boldsymbol{E})^2 - \boldsymbol{b}_p^{\top}\boldsymbol{Q}\boldsymbol{b}_p \tag{28}$$

With:

$$\tilde{\boldsymbol{E}} = det\,(\boldsymbol{E})\boldsymbol{E}^{-1} \tag{29}$$
$$\boldsymbol{E} = 2\boldsymbol{R}_{b,2D}\boldsymbol{D}\boldsymbol{B}^{-1}\boldsymbol{R}_{b,2D}^{T}\boldsymbol{Q}$$

Among the four solutions of Eq. (28) there are two real local minima and two local maxima (depending on the polynomial coefficients) in terms of equivalent Δv. Once ν is known, the initial costates can be derived following backwards the shown passages.

Considering the North-South forced control direction, the procedure is like the one described above. The main difference lies in the control acceleration $\boldsymbol{a}_c = a_{max}\epsilon\boldsymbol{u}_{NS}$, where $\boldsymbol{u}_{NS} = [0\ 0\ 1]^{\top}$ in the ECI reference.

The Hamiltonian-minimising value of ϵ brings to the new control acceleration, which changes Eq. (16) as follows:

$$\dot{\boldsymbol{v}} = \frac{\mu}{r^3}\boldsymbol{r} - a_{max}\boldsymbol{\lambda}_v(\boldsymbol{3})\boldsymbol{u}_{NS} \tag{30}$$

Considering now the East-West control case, $\boldsymbol{a}_c = \boldsymbol{a}_{max}\epsilon\boldsymbol{u}_{EW}$, where $\boldsymbol{u}_{EW} = \frac{\boldsymbol{v}}{v}$ is the velocity unit vector direction. Therefore, the resulting IVP differs from Eq. (16) only in terms of:

$$\dot{\boldsymbol{v}} = \frac{\mu}{r^3}\boldsymbol{r} - \left(\boldsymbol{\lambda}_v \cdot \frac{\boldsymbol{v}}{v}\right)\frac{\boldsymbol{v}}{v} \tag{31}$$

$$\dot{\boldsymbol{\lambda}_v} = -\boldsymbol{\lambda}_r + 2a_{max}\left(\frac{\boldsymbol{\lambda}_v \cdot \boldsymbol{v}}{v^2} - \left(\frac{\boldsymbol{\lambda}_v \cdot \boldsymbol{v}}{v^2}\right)^2 \boldsymbol{v}\right) \tag{32}$$

3. MPBVP for combined CAM and SK

This section presents an integrated strategy to optimize both the CAM and a station-keeping maneuver. The proposed solution reduces the problem to an MPBVP, solved with two different approaches detailed hereafter. Considering the framework described at the beginning of Sect. 1.1, the station-keeping box limits are imposed equal to $\pm 0.05°$ for both latitude and longitude, in agreement with [5]. Moreover, when the primary object is in proximity to one of the box boundaries as depicted in Fig. 1, it is steered to the opposite side as sketched in Fig. 2. This technique is coarse and more operative SK routines will be envisaged in future works. The underlying idea is just to show the method effectiveness.

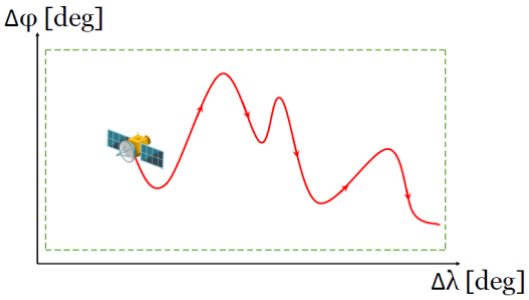

Fig. 1 Satellite motion on its nominal orbit.

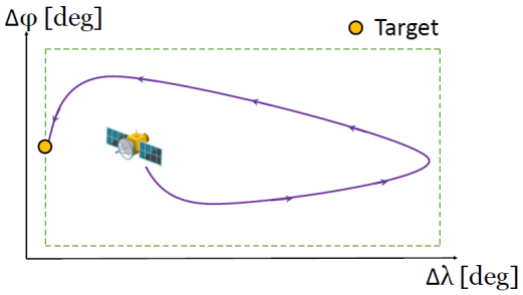

Fig. 2: Satellite motion after station keeping

It is worth noticing that no path constraints are on the trajectory, which may not respect the box for the entire maneuver.

Up to this point, all the quantities considered have been defined in two reference systems: ECI and B-Plane.

However, they are not ideal for the satellite latitude and longitude variations defined in the Earth-Centered Equatorial Frame (ECEF). ECI is inertial, while ECEF rotates with the object. Notably, calling the reference ECEF is an abuse of notation, being tied to the nominal satellite motion without accounting for long-period equator plane perturbations

The rotation matrix to pass from one reference to the other is time-dependent. At the time instant t_0 associated with the definition of the primary and secondary objects' orbits, the two frames deviate from each other by an initial angular offset, labelled with α that linearly increases over time. Therefore, the rotation matrix between ECI and ECEF reference frames is:

$$\boldsymbol{R}_{eci2ecef}(t) = \begin{bmatrix} R_{11}(t) & R_{12}(t) & 0 \\ R_{21}(t) & R_{22}(t) & 0 \\ 0 & 0 & 1 \end{bmatrix} \tag{33}$$

$$\begin{aligned} R_{11}(t) &= R_{22}(t) = cos\big(\omega_p(t-t_0)+\alpha\big) \\ R_{12}(t) &= sin\big(\omega_p(t-t_0)+\alpha\big) \\ R_{21}(t) &= -sin\big(\omega_p(t-t_0)+\alpha\big) \end{aligned} \tag{34}$$

ω_p is the primary object angular velocity. Furthermore, the latitude and longitude variations, $\Delta\alpha$ and $\Delta\lambda$, are evaluated as:

$$\begin{aligned} \Delta\alpha &= \alpha - \alpha_p \\ \Delta\lambda &= \lambda - \lambda_p \end{aligned} \tag{35}$$

where, α_p and λ_p are the reference angles for the latitude and longitude at t_0 respectively, while α and λ are the latitude and longitude of each point along the orbits.

3.1. Energy Sub-Optimal MPBVP for combined CAM and SK

In Fig. 3 the sub-optimal MPBVP formulation is represented. The orange line is the first trajectory segment linked to CAM execution, while the light blue one is associated to station-keeping.

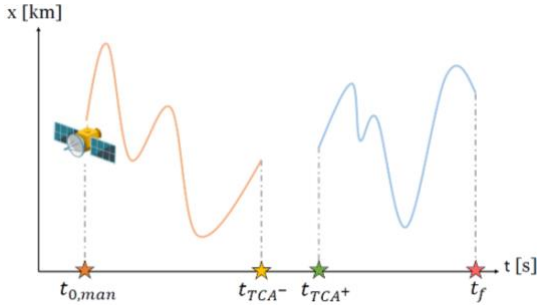

Fig. 3: Two trajectory segments representation

The employed dynamics is reported in Eq. (9) encompassing up to the J_{22} term, while the cost function to minimize changes as follows:

$$J = k\Upsilon(\boldsymbol{r}_{TCA}) + \int_{t_0}^{t_f} \frac{1}{2} a_{max} \boldsymbol{u}^T \boldsymbol{u} dt \tag{36}$$

where Υ is the terminal function representing the inequality constraint on the SMD at t_{TCA}

$$\Upsilon(\boldsymbol{r}_{TCA}^m) = \overline{SMD} - SMD(\boldsymbol{r}_{TCA}^m) \leq 0 \tag{37}$$

Additionally, at t_f the primary must target a desired state coinciding with a suitable point on the station keeping box:

$$\begin{cases} \boldsymbol{r}(t_f) = \boldsymbol{r}_f^m \\ \boldsymbol{v}(t_f) = \boldsymbol{v}_f^m \end{cases} \tag{38}$$

The first solution approach identifies two different cost functions:

$$J_1 = \int_{t_0}^{t_{TCA^-}} \frac{1}{2} a_{max} \boldsymbol{u}^T \boldsymbol{u} dt \tag{39}$$

$$J_2 = k\Upsilon(\boldsymbol{r}_{TCA}) + \int_{t_{TCA^+}}^{t_f} \frac{1}{2} a_{max} \boldsymbol{u}^T \boldsymbol{u} dt \tag{40}$$

After having derived the stationary conditions for both by imposing the state continuity at the conjunction point, the IVP reads:

$$\begin{cases} \dot{\boldsymbol{r}} = \boldsymbol{v} \\ \dot{\boldsymbol{v}} = -\dfrac{\mu}{r^3}\boldsymbol{r} + \boldsymbol{a}_{geo} - a_{max}\boldsymbol{\lambda}_v \\ \dot{\boldsymbol{\lambda}_r} = f\big(\boldsymbol{\lambda}, \omega_p, \boldsymbol{r}, \phi, t, t_0\big) \\ \dot{\boldsymbol{\lambda}_v} = -\boldsymbol{\lambda}_r \end{cases} \tag{41}$$

$$\begin{cases} \boldsymbol{r}(t_0) = \boldsymbol{r}_0^m \\ \boldsymbol{v}(t_0) = \boldsymbol{v}_0^m \\ \boldsymbol{\lambda}_r(t_0) = \boldsymbol{\lambda}_{r_0}^m \\ \boldsymbol{\lambda}_v(t_0) = \boldsymbol{\lambda}_{v_0}^m \end{cases}$$

The initial costates, $\boldsymbol{\lambda}_{r_0^m}$ and $\boldsymbol{\lambda}_{v_0^m}$, can be determined by means of two STMs:

$$\delta \boldsymbol{x}_{TCA^-} = \tilde{\boldsymbol{\Phi}} \delta \boldsymbol{x}_0 \tag{42}$$

$$\delta \boldsymbol{x}_f = \boldsymbol{\Phi} \delta \boldsymbol{x}_{TCA^+} \tag{43}$$

together with some boundary conditions:

$$\begin{aligned} &\boldsymbol{r}(t_0) = \boldsymbol{r}_0^m \\ &\boldsymbol{v}(t_0) = \boldsymbol{v}_0^m \\ &\boldsymbol{\lambda}_{r_{TCA^+}^m} = -k \frac{\partial \Upsilon(\boldsymbol{r})}{\partial \boldsymbol{r}}\bigg|_{r_{TCA}^m} \\ &\boldsymbol{\lambda}_{v_{TCA^+}^m} = \boldsymbol{0} \\ &\boldsymbol{r}_{TCA^-}^m = \boldsymbol{r}_{TCA^+}^m = \boldsymbol{r}_{TCA}^m \\ &\boldsymbol{v}_{TCA^-}^m = \boldsymbol{v}_{TCA^+}^m = \boldsymbol{v}_{TCA}^m \\ &\boldsymbol{r}(t_f) = \boldsymbol{r}_f^m \\ &\boldsymbol{v}(t_f) = \boldsymbol{v}_f^m \end{aligned} \tag{44}$$

$\tilde{\boldsymbol{\Phi}}$ is associated to the first trajectory segment, and $\boldsymbol{\Phi}$ refers to the second one. $\boldsymbol{\delta v_f}$ and $\boldsymbol{\delta r_f}$ are known a priori because they represent the difference of the targeted state with respect to the ballistic trajectory one at t_f . Moreover, $\Upsilon(\boldsymbol{r}_{TCA}) \leq 0$ turns into the following conditions:

$$\begin{cases} k \geq 0 \\ k\Upsilon = 0 \end{cases} \tag{45}$$

To compute $\delta \boldsymbol{r}_{TCA}$, take the first two rows of Eq. (43) :

$$\delta \boldsymbol{r}_{TCA} = \boldsymbol{\eta} + \boldsymbol{F}\boldsymbol{\lambda}_{v^m_{TCA^+}} \tag{46}$$

With:

$$\begin{aligned} \boldsymbol{F} &= -\widetilde{\boldsymbol{A}}\boldsymbol{D} \\ \boldsymbol{E} &= -\widetilde{\boldsymbol{A}}\boldsymbol{B} \\ \boldsymbol{B} &= \boldsymbol{\phi_{22}}\boldsymbol{\phi_{12}^{-1}} \\ \boldsymbol{D} &= \boldsymbol{\phi_{23}} - \boldsymbol{\phi_{22}}\boldsymbol{\phi_{12}^{-1}}\boldsymbol{\phi_{13}} \\ \widetilde{\boldsymbol{A}} &= \boldsymbol{A^{-1}} \\ \boldsymbol{A} &= \boldsymbol{\phi_{21}} - \boldsymbol{\phi_{22}}\boldsymbol{\phi_{12}^{-1}}\boldsymbol{\phi_{11}} \\ \boldsymbol{\eta} &= \widetilde{\boldsymbol{A}}\delta \boldsymbol{v}_f + \boldsymbol{E}\delta \boldsymbol{r}_f \end{aligned} \tag{47}$$

Similarly to the only CAM case, the problem reduces to a system of equations:

$$\begin{cases} \delta \boldsymbol{r}_{TCA} = \boldsymbol{\eta} + \\ -2k\boldsymbol{F}\boldsymbol{R}_{b,2D}^{\top}\boldsymbol{Q}\boldsymbol{R}_{b,2D}(\boldsymbol{r}^m_{TCA} - \boldsymbol{r}_s) \\ k(\boldsymbol{r}^m_{TCA} - \boldsymbol{r}_s)^{\top}\boldsymbol{R}_{b,2D}^{\top}\boldsymbol{Q}\boldsymbol{R}_{b,2D}(\boldsymbol{r}^m_{TCA} - \boldsymbol{r}_s) \\ = k\overline{SMD} \end{cases} \tag{48}$$

Where:

$$\boldsymbol{Q} = \boldsymbol{C^{-1}} \tag{49}$$

Solving Eq. (48), it results in a fifth-order polynomial:

$$\begin{aligned} k\left[k^2(\widetilde{\boldsymbol{P}}\boldsymbol{u})^{\top}\boldsymbol{Q}(\widetilde{\boldsymbol{P}}\boldsymbol{u}) - k\left[\boldsymbol{u}^{\top}\boldsymbol{Q}\widetilde{\boldsymbol{P}}\boldsymbol{u} + (\widetilde{\boldsymbol{P}}\boldsymbol{u})^{\top}\boldsymbol{Q}\boldsymbol{u}\right] + \boldsymbol{u}\boldsymbol{Q}\boldsymbol{u}\right. \\ \left. - \overline{SMD}\, det(I - k\boldsymbol{P})^2\right] = 0 \end{aligned} \tag{50}$$

Where:

$$\begin{aligned} \widetilde{\boldsymbol{P}} &= det\,(\boldsymbol{P})\boldsymbol{P^{-1}} \\ \boldsymbol{P} &= -\boldsymbol{2}\boldsymbol{R}_{b,2D}\boldsymbol{D}\boldsymbol{B^{-1}}\boldsymbol{R}_{b,2d}^{T}\boldsymbol{Q} \\ \boldsymbol{u} &= \boldsymbol{q} + \boldsymbol{b_p} \\ \boldsymbol{b_p} &= \boldsymbol{R}_{b,2D}(\boldsymbol{r}_{TCA} - \boldsymbol{r}_s) \\ \boldsymbol{q} &= \boldsymbol{R_{b,2D}}\boldsymbol{\eta} \end{aligned} \tag{51}$$

In particular, the equation in k has five solutions. The trivial one is $k = 0$, then there are four non null solutions arranged in ascending order. For $k = 0$, the SMD inequality must be verified with the obtained linear relations (no integration needed). Analysing each case separately:

- If $\Upsilon \leq 0$, the spacecraft motion exploits only the perturbation from the thrusters before TCA. Therefore, $\boldsymbol{\lambda}_{r^m_{TCA^+}} = \boldsymbol{\lambda}_{v^m_{TCA^+}} = 0$.
- If $\Upsilon > 0$ holds, $\boldsymbol{\lambda}_{r^m_{TCA^+}}$ can be retrieved by selecting one solution for $k \neq 0$, either correspong to a minima or a maxima, whereas $\boldsymbol{\lambda}_{v^m_{TCA^+}}$ is still null.

Eventually, the initial costates are:

$$\begin{cases} \boldsymbol{\lambda}_{r^m_0} = \widetilde{\boldsymbol{E}}^{\boldsymbol{-1}}\left(\delta \boldsymbol{v}_{TCA} - \widetilde{\boldsymbol{F}}\delta \boldsymbol{r}_{TCA}\right) \\ \boldsymbol{\lambda}_{v^m_0} = \widetilde{\boldsymbol{B}}\delta \boldsymbol{r}_{TCA} + \widetilde{\boldsymbol{D}}\widetilde{\boldsymbol{E}}^{\boldsymbol{-1}}\left(\delta \boldsymbol{v}_{TCA} - \widetilde{\boldsymbol{F}}\delta \boldsymbol{r}_{TCA}\right) \end{cases} \tag{52}$$

Where:

$$\begin{aligned} \widetilde{\boldsymbol{E}} &= \widetilde{\boldsymbol{\phi}}_{23} + \widetilde{\boldsymbol{\phi}}_{24}\widetilde{\boldsymbol{D}} \\ \widetilde{\boldsymbol{F}} &= \widetilde{\boldsymbol{\phi}}_{24}\widetilde{\boldsymbol{B}} \\ \widetilde{\boldsymbol{B}} &= \widetilde{\boldsymbol{\phi}}^{\boldsymbol{-1}}_{\boldsymbol{14}} \\ \widetilde{\boldsymbol{D}} &= -\widetilde{\boldsymbol{B}}\widetilde{\boldsymbol{\phi}}_{13} \\ \boldsymbol{v}^m_{TCA} - \boldsymbol{v}_{TCA} &= \boldsymbol{Y}\delta \boldsymbol{r}_f + \boldsymbol{\Omega}\delta \boldsymbol{r}_{TCA} + \\ &\quad + \boldsymbol{\Pi}\boldsymbol{\lambda}_{r^m_{TCA^+}} \\ \boldsymbol{Y} &= \widetilde{\boldsymbol{\phi}}^{\boldsymbol{-1}}_{\boldsymbol{12}} \\ \boldsymbol{\Omega} &= \widetilde{\boldsymbol{\phi}}^{\boldsymbol{-1}}_{\boldsymbol{12}}\widetilde{\boldsymbol{\phi}}_{11} \\ \boldsymbol{\Pi} &= \widetilde{\boldsymbol{\phi}}^{\boldsymbol{-1}}_{\boldsymbol{12}}\widetilde{\boldsymbol{\phi}}_{13} \end{aligned} \tag{53}$$

3.2. Energy Optimal MPBVP for combined CAM and SK

However, the quantities derived at t_{TCA} are not influenced by those at t_0. Indeed, this problem does not jointly optimize CAM and station-keeping. An alternative method, called optimal MPBVP, instead only employs one cost function for the entire from t_0 to t_f.

The main difference concerning the previous solution scheme is in the stationarity conditions. The constraints mirror the ones of the combined suboptimal CAM and SK except for the costates at TCA:

$$2k\frac{\partial \Upsilon}{\partial \boldsymbol{x}_{TCA}} + \boldsymbol{\lambda}_{TCA^+} + \boldsymbol{\lambda}_{TCA^-} = 0 \tag{54}$$

Adopting the same notation for the STM representation in the two branches, Express$\boldsymbol{\lambda}_{r^m_0}$ and $\boldsymbol{\lambda}_{v^m_0}$ as a function of $\delta \boldsymbol{r}_{TCA}$ and $\delta \boldsymbol{v}_{TCA}$ by means of the first and the second rows of Eq. (42):

$$\begin{cases} \boldsymbol{\lambda}_{r^m_0} = \boldsymbol{U}\delta \boldsymbol{r}_{TCA} + \boldsymbol{V}\delta \boldsymbol{v}_{TCA} \\ \boldsymbol{\lambda}_{v^m_0} = \boldsymbol{T}\delta \boldsymbol{r}_{TCA} + \boldsymbol{S}\delta \boldsymbol{v}_{TCA} \end{cases} \tag{55}$$

With:

$$\begin{aligned}
&\boldsymbol{S} = \boldsymbol{M}^{-1} \\
&\boldsymbol{V} = \boldsymbol{KS} \\
&\boldsymbol{U} = (\boldsymbol{Q} + \boldsymbol{KT}) \\
&\boldsymbol{T} = -\boldsymbol{M}^{-1}\boldsymbol{N} \\
&\boldsymbol{M} = \widetilde{\boldsymbol{\phi}}_{23}\boldsymbol{K} + \boldsymbol{K}\widetilde{\boldsymbol{\phi}}_{24} \\
&\boldsymbol{N} = \widetilde{\boldsymbol{\phi}}_{23}\boldsymbol{Q} \\
&\boldsymbol{K} = \widetilde{\boldsymbol{\phi}}_{23}^{-1}\widetilde{\boldsymbol{\phi}}_{14} \\
&\boldsymbol{Q} = \widetilde{\boldsymbol{\phi}}_{13}^{-1}
\end{aligned} \tag{56}$$

The third and the forth rows of Eq. (42) lead to $\boldsymbol{\lambda}_{r_{TCA^-}^m}$ and $\boldsymbol{\lambda}_{v_{TCA^-}^m}$ dependent on $\delta\boldsymbol{r}_{TCA}$ and $\delta\boldsymbol{v}_{TCA}$:

$$\begin{cases}
\boldsymbol{\lambda}_{r_{TCA^-}^m} = \boldsymbol{L}\delta\boldsymbol{r}_{TCA} + \boldsymbol{O}\delta\boldsymbol{v}_{TCA} \\
\boldsymbol{\lambda}_{v_{TCA^-}^m} = \widetilde{\boldsymbol{T}}\delta\boldsymbol{r}_{TCA} + \widetilde{\boldsymbol{U}}\delta\boldsymbol{v}_{TCA}
\end{cases} \tag{57}$$

With:

$$\begin{aligned}
&\boldsymbol{L} = \widetilde{\boldsymbol{\phi}}_{33}\boldsymbol{U} + \widetilde{\boldsymbol{\phi}}_{34}\boldsymbol{T} \\
&\boldsymbol{O} = \widetilde{\boldsymbol{\phi}}_{33}\boldsymbol{V} + \widetilde{\boldsymbol{\phi}}_{34}\boldsymbol{S} \\
&\widetilde{\boldsymbol{U}} = \widetilde{\boldsymbol{\phi}}_{43}\boldsymbol{U} + \widetilde{\boldsymbol{\phi}}_{44}\boldsymbol{T} \\
&\widetilde{\boldsymbol{T}} = \widetilde{\boldsymbol{\phi}}_{43}\boldsymbol{V} + \widetilde{\boldsymbol{\phi}}_{44}\boldsymbol{S}
\end{aligned} \tag{58}$$

Successively, the first and the second rows of Eq. (43) , and Eq. (54) are leveraged to express $\delta\boldsymbol{r}_f$ and $\delta\boldsymbol{v}_f$ as a function of $\boldsymbol{r}_{TCA}^m$ and $\boldsymbol{v}_{TCA}^m$:

$$\begin{aligned}
\delta\boldsymbol{r}_f &= \widetilde{\boldsymbol{W}}\delta\boldsymbol{r}_{TCA} + \widetilde{\boldsymbol{Z}}\delta\boldsymbol{v}_{TCA} + \\
&\quad -k\widetilde{\boldsymbol{A}}\boldsymbol{R}_{\boldsymbol{b,2D}}(\boldsymbol{r}_{TCA}^m - \boldsymbol{r}_s) \\
\delta\boldsymbol{v}_f &= \boldsymbol{H}\delta\boldsymbol{r}_{TCA} + \boldsymbol{X}\delta\boldsymbol{r}_{TCA} + \\
&\quad - k\boldsymbol{J}\boldsymbol{R}_{\boldsymbol{b,2D}}(\boldsymbol{r}_{TCA}^m - \boldsymbol{r}_s)
\end{aligned} \tag{59}$$

Where:

$$\begin{aligned}
&\widetilde{\boldsymbol{W}} = \boldsymbol{W} + \boldsymbol{\phi}_{\boldsymbol{13}}\boldsymbol{L} \\
&\widetilde{\boldsymbol{Z}} = \boldsymbol{Z} + \boldsymbol{\phi}_{\boldsymbol{13}}\boldsymbol{O} \\
&\widetilde{\boldsymbol{A}} = -\boldsymbol{4}\boldsymbol{\phi}_{\boldsymbol{13}}\boldsymbol{R}_{\boldsymbol{b,2D}}^{\boldsymbol{T}}\boldsymbol{Q} \\
&\boldsymbol{Z} = \boldsymbol{\phi}_{\boldsymbol{12}} + \boldsymbol{\phi}_{\boldsymbol{14}}\widetilde{\boldsymbol{T}} \\
&\boldsymbol{W} = \boldsymbol{\phi}_{\boldsymbol{11}} + \boldsymbol{\phi}_{\boldsymbol{14}}\widetilde{\boldsymbol{U}} \\
&\boldsymbol{H} = \boldsymbol{\phi}_{\boldsymbol{21}} + \boldsymbol{\phi}_{\boldsymbol{22}}\boldsymbol{F} + \boldsymbol{\phi}_{\boldsymbol{23}}(\boldsymbol{L} + \boldsymbol{OF}) + \\
&\boldsymbol{\phi}_{\boldsymbol{24}}\big(\widetilde{\boldsymbol{U}} + \widetilde{\boldsymbol{T}}\boldsymbol{F}\big) \\
&\boldsymbol{X} = \boldsymbol{\phi}_{\boldsymbol{22}}\boldsymbol{E} + \boldsymbol{\phi}_{\boldsymbol{23}}\,\boldsymbol{OE} + \boldsymbol{\phi}_{\boldsymbol{24}}\widetilde{\boldsymbol{T}}\boldsymbol{E} \\
&\boldsymbol{J} = \boldsymbol{\phi}_{\boldsymbol{22}}\boldsymbol{G} + \boldsymbol{\phi}_{\boldsymbol{23}}\left(-\boldsymbol{4}\boldsymbol{R}_{\boldsymbol{b,2D}}^{\boldsymbol{T}}\boldsymbol{Q} + \right. \\
&\left.\boldsymbol{OG}\right) + \boldsymbol{\phi}_{\boldsymbol{24}}\widetilde{\boldsymbol{T}}\boldsymbol{G} \\
&\boldsymbol{F} = -\boldsymbol{E}\widetilde{\boldsymbol{W}} \\
&\boldsymbol{G} = -\boldsymbol{E}\widetilde{\boldsymbol{A}} \\
&\boldsymbol{E} = \widetilde{\boldsymbol{Z}}^{-1}
\end{aligned} \tag{60}$$

$\delta\boldsymbol{r}_{TCA}$ is then:

$$\delta\boldsymbol{r}_{TCA} = \boldsymbol{u} + \boldsymbol{kP}\boldsymbol{R}_{\boldsymbol{b,2D}}(\boldsymbol{r}_{TCA}^m - \boldsymbol{r}_s) \tag{61}$$

With:

$$\begin{aligned}
&\boldsymbol{u} = \boldsymbol{H}^{-1}\big(\delta\boldsymbol{v}_f - \boldsymbol{X}\delta\boldsymbol{r}_f\big) \\
&\boldsymbol{P} = \boldsymbol{H}^{-1}\boldsymbol{J}
\end{aligned} \tag{62}$$

From here the steps match the ones from Eq. (48) to Eq. (50).

Again, there are five solutions, and analogously to the previous case $k = 0$ is the trivial one, while the others are stored in ascending order.

If the solution $k = 0$ is picked, the condition on the SMD must be verified. Therefore:

- If $\Upsilon \leq 0$, the maneuver is a pure station-keeping, because $\boldsymbol{\lambda}_{r_{TCA^+}^m} = \boldsymbol{\lambda}_{r_{TCA^-}^m}$, so there are no discontinuities. Station-keeping automatically satisfies the SMD inequality.
- If $\Upsilon > 0$, the equality condition on the SMD enforces selecting one of the solutions different from zero, preferably a minimum.

$\boldsymbol{\lambda}_{r_0^m}$ and $\boldsymbol{\lambda}_{v_0^m}$ are derived by following the procedure backwards computing $\delta\boldsymbol{r}_{TCA}$ and $\delta\boldsymbol{v}_{TCA}$.
Where:

$$\begin{aligned}
\delta\boldsymbol{v}_{TCA} = \boldsymbol{E}\delta\boldsymbol{r}_f + \boldsymbol{F}\delta\boldsymbol{r}_{TCA} + \\
+k\,\boldsymbol{G}\boldsymbol{R}_{\boldsymbol{b,2D}}(\boldsymbol{r}_{TCA}^m - \boldsymbol{r}_s)
\end{aligned} \tag{63}$$

4. Results

The case under study in the GEO regime for the implementation of the EOP is depicted in Fig. 4. The Keplerian parameters of the two orbits are reported in Table 1 and Table 2.

a [km]	**e** [-]	**i** [deg]	$\boldsymbol{\Omega}$ $[deg]$	$\boldsymbol{\omega}$ [deg]
42220	0	1.55e-4	158.04	315.00

Table 1: Primary object orbital elements.

Notably, the secondary object is a rocket body from the catalogue in [6] left in an Extended Geostationary Orbit (EGO).

a [km]	**e** [-]	**i** [deg]	$\boldsymbol{\Omega}$ $[deg]$	$\boldsymbol{\omega}$ [deg]
42254	3.23e-4	13.73	23.04	102.97

Table 2: Secondary object orbital elements.

$\overline{\boldsymbol{PoC}}$	$\overline{\boldsymbol{SMD}}$
8.4768e-6	10

Table 3: PoC and SMD imposed threshold.

The SMD and PoC thresholds are summarized in Table 3.

4.1. Energy Optimal CAM for free, E-W and N-S thrust directions

For the first three firing strategies in case of only CAM, the time range for the firing window ($\Delta\theta$) goes from 0.1 to 1.5 orbits before conjunction.

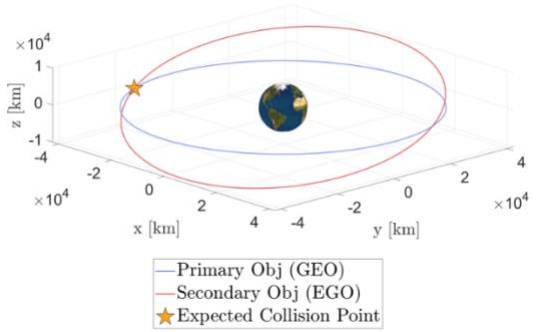

Fig. 4: Study case with the primary object belonging to GEO and the secondary object belonging to and Extended Geostationary Orbit (EGO).

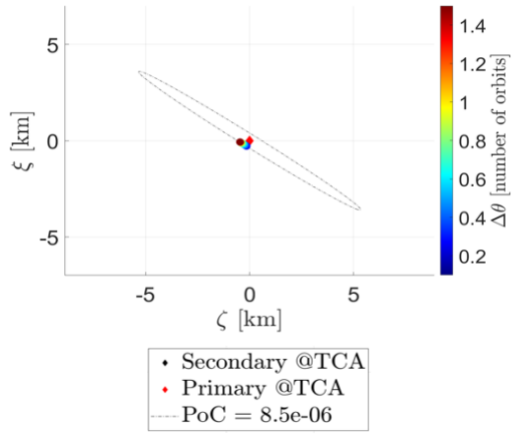

Fig. 5: B-Plane for the free-direction control case.

The primary object position after the CAM in the B-Plane reference together with the PoC ellipse is reported in Fig. 5. Moreover, the Δv contribution, the control acceleration, $\boldsymbol{\lambda}_v$, the PoC, and the computational time are studied. The Δv in Fig. 6 is like the one for the East-West case, while for the North-South one it is less smooth and one order of magnitude larger. As expected, in the free-direction and East-West control cases, the control acceleration transverse component turns to be the largest far from conjunction, while in the North-South case it is the out-of-plane one. The $\boldsymbol{\lambda}_v$ time evolution is similar in the three cases, but with different orders of magnitude. The largest deviation between the real and expected PoC is in the North-South case, 10^{-7}, otherwise it stays around 10^{-10}. Lastly, the computational ranges from 0.1s to 1 s, in line with the propagation time windows duration. The computational performances in Matlab© are assessed with an Asus ZenBook notebook equipped with Intel CORE i7 10th generation, with a base frequency equal to 1.80 GHz and 2.30 GHz in single core, 8.00 Gb of RAM, and 4 cores.

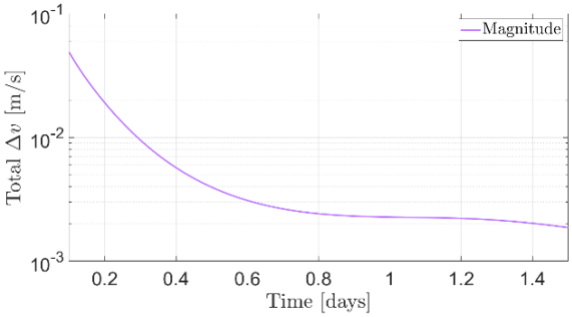

Fig. 6: Required Δv for the maneuver execution for the free-direction control case.

4.2. MPBVP for combined CAM and SK

For the sub-optimal MPBVP, the extrapolated results refer to the solution $k = 0$ of Eq. (50); while for the optimal MPBVP the results are obtained both with $k = 0$ and $k \neq 0$. However, after a filtering procedure as explained hereafter, only the maneuvers with $k = 0$ are visible, because the others exceed the imposed thresholds. Usually, station-keeping is enough to satisfy the PoC constraint at TCA. Differently, both CAM and station-keeping are executed with $k \neq 0$. Indeed, the MPBVP allows understanding a priori if CAM is necessary or not, leading to a better problem optimization. Two propagation time vectors, T_{back} and T_{after}, from 0.1 to 1.5 days are considered before and after the conjunction, respectively.

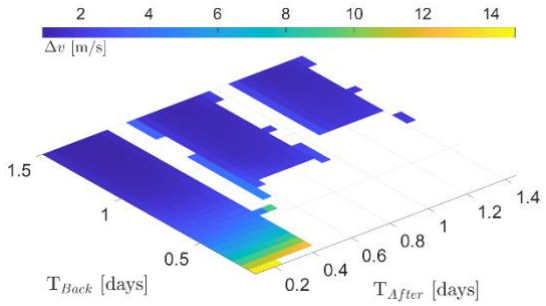

Fig. 7:Δv surface for the sub-optimal MPBVP.

The B-Plane final position of the primary object, the estimated Δv and final position targeting surfaces are reported. In both sub-optimal and optimal scenarios, the points in B-Plane land far away from the iso-probability ellipse (the SMD inequality is fulfilled). Fig. 7 portrays the Δv for the sub-optimal MPBVP.

The white-coloured areas are related to pairs of T_{after} and T_{back} requiring a Δv demand larger than 15 m/s not compatible with low-thrust propulsion.

Fig. 8 shows the accuracy of the sub-optimal method in targeting the imposed final position. A filter is applied to discard the combinations of T_{after} and T_{back} producing an error larger than 1 km or Δv greater than 15 m/s. Similar graphs are obtained for the optimal solution approach. Fig. 9 illustrates the Δv and the final position error with respect to the target position for the optimal MPBVP, respectively. The main difference is the reduced, white-coloured regions of Fig. 9 when compared to Fig. 7, being globally optimized.

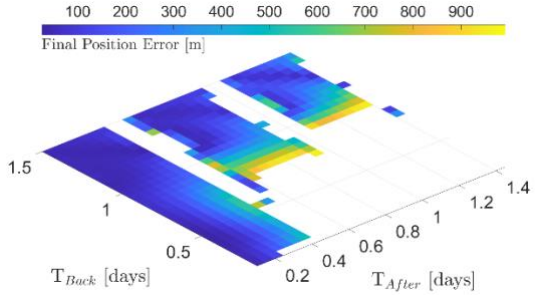

Fig. 8: Error on the targeting of the final point for the sub-optimal MPBVP solution.

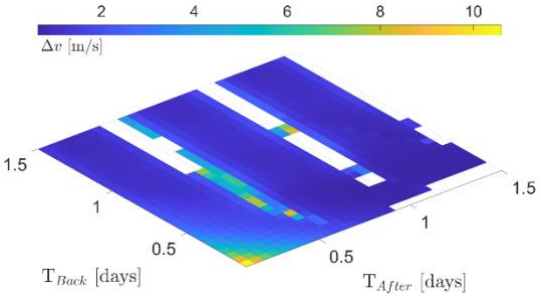

Fig. 9: Δv surface for the optimal MPBVP solution.

The solution aims to reduce the Probability of Collision between the primary and the secondary objects as well as to keep the controlled satellite inside the assigned box. Fig. 11 renders the final position in the B-Plane reference of the primary object ($\boldsymbol{b}_f$), without applying the filtering mentioned above.

Notably, not all the solutions are identified with $k = 0$, but some of them are characterized by $k \neq 0$ and target the probability ellipse because of the CAM execution. However, these points are not visible after screening because they relate to values of Δv or error in targeting the final position larger than 15 m/s or 1 km, respectively.

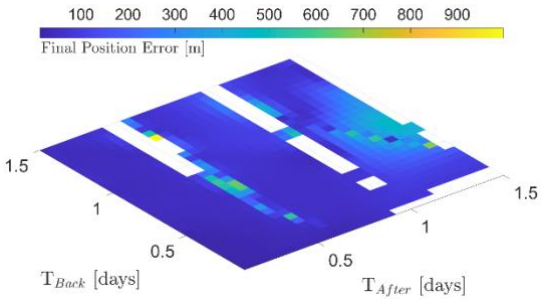

Fig. 10: Error on the targeting of the final point for the optimal MPBVP solution.

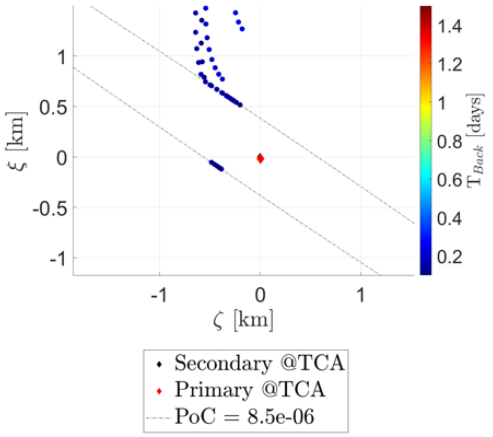

Fig. 11: Zoomed B-Plane for the optimal MPBVP without applying the filtering.

Hereafter, the condition of station-keeping with the minimum Δv required derived from the optimal MPBVP is briefly analysed looking at the most relevant quantities related to the maneuver execution.

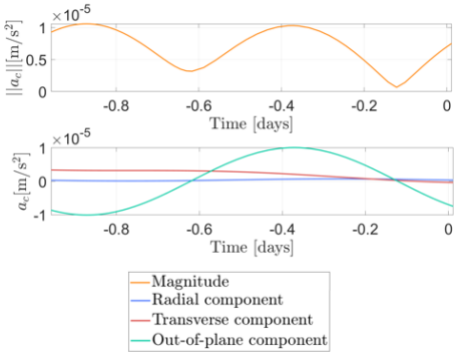

Fig. 12: Control Acceleration from t_0 to t_{TCA} for the optimal MPBVP solution with box respected and minimum Δv required.

The first quantity to look at is the control acceleration. Its evolution is reported in Fig. 12, in magnitude and components terms from t_0 to t_{TCA}.

In this case the out-of-plane direction is predominant.

Fig. 13 depicts instead the tendency of the control acceleration from conjunction (t_{TCA}) to the final time of the maneuver (t_f).

As it can be noticed, the behaviour of the control acceleration during the two propagations is very similar.

Moreover, both the order of magnitudes agrees with the low-thrust propulsion technology maximum allowed values.

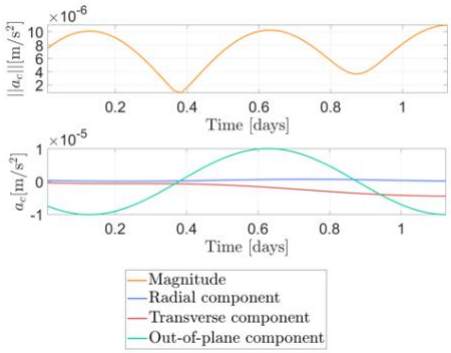

Fig. 13: Control acceleration from t_0 to t_{TCA} for the optimal MPBVP solution with box respected and minimum Δv required.

Looking Fig. 14 and Fig. 15, it represents the primary object trajectory evolution concerning the assigned box.

In particular, Fig. 14 depicts the three-dimensional representation of the controlled body trajectory.

The object relative position is characterized by a radial and out-of-plane and transversal motion.

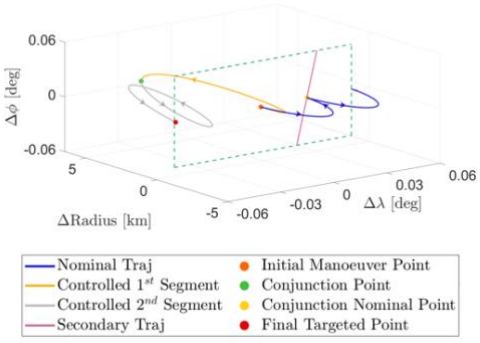

Fig. 14: 3D station-keeping box optimal MPBVP solution with box respected and minimum Δv required.

In addition, Fig. 15 confirms that the primary body respects the assigned box for the entire duration of the maneuver with the minimum cost for the supplied Δv.

For the sake of completeness, the computational time is investigated also for the solution of the MPBVPs. It results higher than in only CAM case, because of the increased dynamics complexity, and it spans from 0.1 to 4 s.

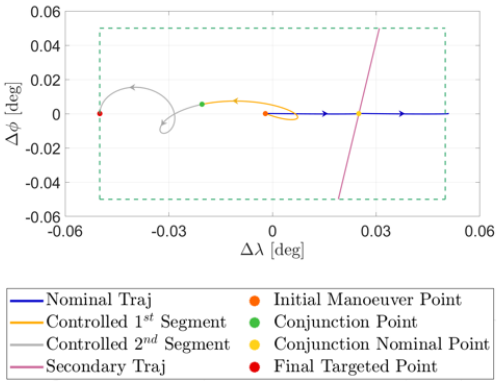

Fig. 15: 2D station-keeping box optimal MPBVP solution with box respected and minimum Δv required.

5. Conclusions

This work started from an already existing CAM control strategy, which has been extended to the Geostationary case through subsequent steps.

First, the only CAM policy employs a pure Keplerian model. Consequently, the required computational time is the smallest, due to lower dynamical complexity. Moreover, it is evident from the graphs that the required Δv is strongly influenced by the time at which the maneuver is executed.

Successively, for the sake of treating a more operative scenario, two Multi-Point Boundary Value Problems that include both CAM and station-keeping have been investigated in presence of the geopotential perturbation, essential for the GEO regime.

In this way, the two trajectory segments can be seen as a unique path from the initial maneuvering point to the imposed final one sticked to the assigned station-keeping box.

When station-keeping alone is enough to satisfy the condition on the probability of collision at the conjunction point, CAM is not performed.

Conversely, both are embedded in a single maneuver with an analytical solution. This represents the focus of the dissertation.

The obtained Δv for the maneuver execution is not always compatible with the limits imposed by the low-thurst propulsion technology.

However, for most of the identified operating points, the Δv demand is below 15 m/s.

Though, there are cases where the required Δv overtake the imposed threshold, so another type of propulsion should be considered.

In conclusion, all the methods have been tested to understand the required computational time using

Matlab© for future on-board implementation. Lastly, some possible developments are proposed hereafter.

From the operative scenario standpoint, a bang-bang firing should be investigated adopting the guess stemmed from EOP formulation. Additionally, for many of the analysed cases, the satellite trajectory violates the station-keeping box during the execution of the manoeuvres. One possible solution could be the implementation of a path constraint. Furthermore, the method developed here could be extended to other orbital regimes (e.g. the cislunar environment), since only hinges on boundary conditions.

In fact, the dynamical model could embed: higher orders for the geopotential, Solar Radiation Pressure and Soli-Lunar gravitational perturbations.

In the event of early maneuvers one may overcome the linear approximation of the dynamics with differential algebra, increasing the overall accuracy with regard to PoC and final target state.

Eventually, One research topic could be the implementation of analytical multi-impulsive strategies.

References

[1] ESA, “Space debris problem,” 2022.

[2] M. F. P. P. D. L. R. A. Andrea De Vittori, “Low-Thrust Collision Avoidance Maneuver Optimization,” Journal of Guidance, Control, and Dynamics, pp. 1-15, 2022.

[3] J. H.-A. a. C. Bombardelli, “Low-thrust collision avoidance in circular orbits,” Jurnal of Guidance, Control, and Dynamics, vol. 44, pp. 983-995, 2021.

[4] I. G. C. C. a. J. Z. L. Li, “Design of Low-thrust control in the geostationary region for station keepin,” 2019.

[5] H. D. K. a. J. S. S. C. Lee, “Collision avoidance maneuver planning using GA for LEO and GEO satellite maintained in keeping area,” International Journal of Aeronautical and Space Sceinces, vol. 13, pp. 474-483, 2012.

[6] “Space track online,” 2022. [Online]. Available: https://www.space-track.org/.